

Vortex phase diagram and temperature-dependent second-peak effect in overdoped $\text{Bi}_2\text{Sr}_2\text{CuO}_{6+\delta}$ crystals

A. Piriou^{1,*}, E. Giannini¹, Y. Fasano^{1†}, C. Senatore¹, and Ø. Fischer¹

¹ *Département de Physique de la Matière Condensée, Université de Genève,
24 Quai Ernest-Ansermet, 1211 Geneva, Switzerland*

(Dated: April 8, 2010)

We study the vortex phase diagram of the single-layer $\text{Bi}_2\text{Sr}_2\text{CuO}_{6+\delta}$ (Bi2201) superconductor by means of bulk magnetization measurements on high-quality oxygen-overdoped crystals. In striking contrast with the results found in the moderately-doped two and three-layer Bi-based cuprates, Bi2201 exhibits a strong temperature-dependent second-peak effect. By means of measurements of the in and out-of-plane first-penetration field we provide direct evidence that this phenomenon is mainly associated to an increase of the electromagnetic anisotropy on warming. The effect of oxygen-doping δ on the vortex phase diagram results in both the irreversibility and second-peak lines shifting to higher temperatures and fields. This enhanced stability of the Bragg glass phase suggests that the interlayer coupling between Cu-O layers increases with δ . In addition, we found that the critical temperature follows the parabolic relation with the number of holes per Cu-O plane that holds for most single and two-layer cuprates.

PACS numbers: 74.72.Hs, 74.62.Dh, 74.25.Dw, 74.25.Ha

Keywords: pure Bi2201 crystals, oxygen-doping, vortex phase diagram

Introduction

In the Bi-based series of superconducting cuprates with the general formula $\text{Bi}_2\text{Sr}_2\text{Ca}_{n-1}\text{Cu}_n\text{O}_{2n+4+\delta}$ ($n=1,2,3$), the single-layer compound $\text{Bi}_2\text{Sr}_2\text{CuO}_6$ (Bi2201) [1] is the less assiduously investigated because of its lower critical temperature $T_c \approx 15$ K and the difficulty of synthesizing the pure superconducting phase. However, this compound offers an excellent tool for directly relating its structural and chemical peculiarities to the electronic properties of the Cu-O layer. Due to the scarcity of pure Bi2201 crystals, studies on its vortex phase diagram are lacking and exhaustive magnetic measurements in the superconducting state are still to be reported. We present here the first magnetic bulk measurements on pure Bi2201 crystals, draw the vortex phase diagram and report its evolution with oxygen content δ in the overdoped regime. In order to do this study, we have grown high-purity and large crystals of Bi2201 (typical areas of 1 to 5 mm²).

In the case of the two and three-layer Bi-based cuprates the vortex liquid phase spans over a considerable fraction of the $H - T$ phase diagram [2, 3]. On cooling at low magnetic fields the vortex matter undergoes a first-order solidification transition at T_m [2, 3]. Upon further cooling the magnetic response becomes irreversible since pinning sets-in at a temperature $T_{IL}(H) \lesssim T_m(H)$, the so-called irreversibility line. In the case of Bi2212 the low-temperature vortex phase exhibits quasi-crystalline order [4–6]. This observation is consistent with the theoretical

proposal that the phase stable at low temperatures is a Bragg glass [7, 8]. When increasing field at low temperatures, an order-disorder transition manifests as the so-called second-peak effect in the irreversible magnetization [9, 10]. This second-peak effect starts at an onset field, H_{ON} , and presents a local maximum at H_{SP} . Recent studies in several cuprates raised the discussion on identifying the order-disorder transition field, H_{OD} , with either the onset field H_{ON} [11, 12] or the inflection point between H_{ON} and H_{SP} located at H_{INF} [14–17]. In the case of moderately-doped Bi2212 and Bi2223 the second-peak maximum H_{SP} is roughly temperature-independent [10, 18, 19].

In this work we report that, unexpectedly, in Bi2201 the second-peak effect strongly depends on temperature. In order to elucidate the origin of this phenomenon we performed a detailed study of the anisotropy parameter, $\gamma = \sqrt{m_c/m_{ab}}$ (the ratio between the effective masses along the c axis and ab plane) and found that it strongly depends on temperature. Such a dependence is the main responsible for the increase of $H_{SP}(T)$, $H_{ON}(T)$ and $H_{INF}(T)$ that we observed in Bi2201 on cooling.

Data on the evolution of the vortex phase diagram with oxygen doping in Bi2201 crystals was also lacking and is reported here for the first time. Variations of the doping level greatly modify the vortex phase diagram of Bi-based cuprates [10, 18–21] mainly by inducing changes in the Cu-O interlayer coupling. In particular, both in Bi2212 and Bi2223, the low-field phase spans up to higher temperatures and fields on increasing δ . This is consistent with the measured decrease of γ (increase of interlayer coupling) with oxygen concentration [10, 19–22]. We found that in Bi2201 the doping-evolution of the irreversibility and second-peak lines are qualitatively similar to those of Bi2212 and Bi2223, suggesting an enhancement of interlayer coupling on increasing δ .

[†]Present address: Instituto Balseiro and Centro Atómico Bariloche, Comisión Nacional de Energía Atómica, Avenida Bustillo 9500, 8400 Bariloche, Argentina

*Electronic address: Alexandre.Piriou@unige.ch

In the case of Bi2212 and Bi2223 the doping-evolution of the superconducting parameters has been thoroughly tracked, spanning from the underdoped (UD) to the overdoped (OD) regime. For the two-layer compound T_c follows a parabolic trend with carrier density [23–25]. The same law is not fulfilled in the three-layer compound presumably due to differences in the doping level of the inner and outer Cu-O layers [19]. Experimental data on tuning the doping level in pure Bi2201 is in short supply and controversial. The difficulties in synthesizing pure Bi2201 have fostered the study of the more easily processed La and/or Pb-doped Bi2201 [26–30]. Presently, the eye has turned back to the pure Bi2201 phase, however only a single work concerning polycrystalline samples reports on the dependence of T_c on doping [31]. Sizeable crystals of Bi2201 have been recently grown [32, 33], but their transition temperatures were not greater than 8 K and the effect of post-annealing treatments on T_c was not clarified [33]. We have been able to tune the doping level over the whole overdoped regime and to achieve a $T_{c,max} = 15$ K, close to the maximum of 16.5 K reported for polycrystalline samples [31]. Furthermore, we report that in our Bi2201 crystals T_c follows a parabolic trend with δ , as in the case of several single and two-layer cuprates [23, 24].

Crystal growth and oxygen-doping

Pure Bi2201 crystals were grown by means of the travelling-solvent floating-zone (TSFZ) method in a home-made two-mirror furnace. Details on the furnace and the growth technique are described in a previous work [34]. In the case of Bi2201 the growth of crystals is favored by starting from an excess of Bi in the nominal composition and by melting in a pure oxygen atmosphere, as previously reported by other authors [32, 33]. The crystals used in our study were grown from a precursor of nominal composition $\text{Bi}_{2.05}\text{Sr}_{1.95}\text{CuO}_{6.025}$. High-purity Bi_2O_3 (99,999%), SrCO_3 (99,999%) and CuO (99,999%) were mixed, milled, and calcined at 780 – 800°C during 100-120 hours in total, with four intermediate manual grindings. The precursor (feed) rod was cold-pressed in a cylindrical mold of about 80 mm in length and 7 mm in diameter and heat-treated in air at 850°C for 36 hours. After a first-zone melting at high travelling-velocity (25 mm/hour), performed with the aim of increasing and homogenizing the density of the feed rod, the slow TSFZ was performed at 0.55 mm/hour under an oxygen overpressure of 2 bar. A crystallized end of a previous sample with the same composition was used as a seed. Crystals with typical lengths of 1-5 mm and thicknesses of 0.1-0.2 mm (see insert of Fig. 1) were cleaved from the core of the crystallized rod.

As-grown crystals are superconducting with an onset of the $\chi'(T)$ transition at 10 K and a transition width of about 4 K. The quality of the crystals was checked by x-ray diffraction (XRD) and energy-dispersive x-ray micro-

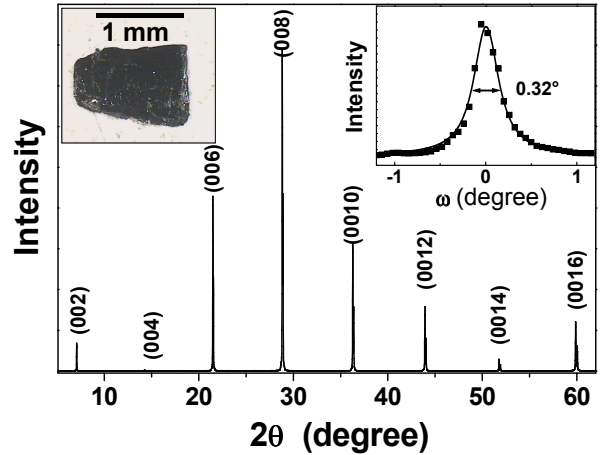


FIG. 1: X-ray diffraction pattern of one of our typical Bi2201 crystals oriented with the c -axis parallel to the scattering vector. Left-hand insert: picture of the crystal. Right-hand insert: rocking-curve exhibiting a full-width at half maximum of 0.32° .

probe (EDX). The XRD pattern measured in a Bragg-Brentano $\theta - 2\theta$ geometry using a $\text{Cu} - K\alpha$ radiation is shown in Fig. 1 ($K\alpha_1 = 1.5406 \text{ \AA}$, $K\alpha_2 = 1.5444 \text{ \AA}$, $\alpha_2/\alpha_1 = 0.5$). In this configuration, only the $[00l]$ planes contribute to the pattern. The rocking curve of the $[006]$ reflection is shown in the right-insert of Fig. 1: the full-width at half maximum is of 0.32° whereas that of the $I(2\theta)$ peaks is typically of the order of 0.05° . This XRD data proves the high crystallinity of our samples. The chemical composition of the crystals was checked by EDX using a Noran Pioneer X-ray detector mounted in a Cambridge 438VP scanning-electron-microscope. The average composition measured over large crystal areas is $\text{Bi}_{2.05}\text{Sr}_{1.98}\text{Cu}_{0.98}\text{O}_{6.04}$ with errors on the local deviations in formula units of $\Delta(\text{Bi}) = 0.05$, $\Delta(\text{Sr}) = 0.05$ and $\Delta(\text{Cu}) = 0.02$.

In order to tune and homogenize the carrier concentration the crystals were annealed during 24 to 48 hours at 500°C, under various oxygen partial-pressures $P(\text{O}_2)$. Annealing treatments longer than 48 hours did not affect either the transition temperature T_c or the transition width ΔT_c . Magnetic susceptibility measurements reveal single and relatively sharp superconducting transitions with widths ranging from 1 to 3.5 K. Examples of superconducting transitions for various doping levels are shown in Fig. 2. T_c is considered as the temperature at which the temperature-derivative of the AC susceptibility, $\partial\chi'/\partial T$, and DC magnetization, $\partial M/\partial T$, are peaked. Figure 3 shows the dependence of T_c/T_c^{max} on $P(\text{O}_2)$ for our Bi2201 crystals. Each point corresponds to at least 5 samples with the same critical temperature within the error. Superconductivity is suppressed when annealing at $P(\text{O}_2) = 400$ bar. As expected [31], after annealing at 500°C Bi2201 is in the overdoped regime and still re-

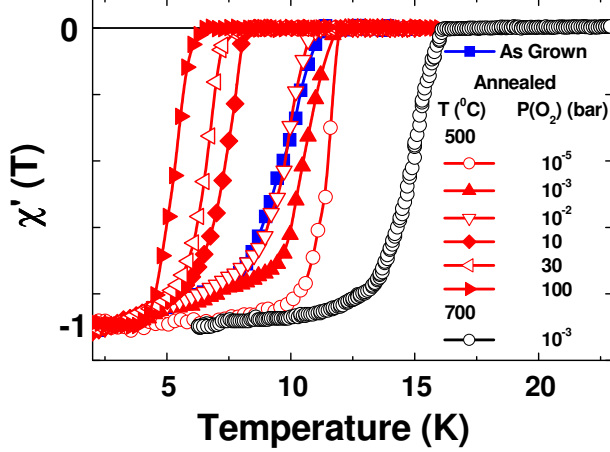


FIG. 2: Real part of the magnetic susceptibility as a function of temperature for our samples of Bi2201 annealed under different oxygen partial-pressures $P(O_2)$. The annealing treatments were performed at 500°C but one at 700°C. The $\chi'(T)$ measurements were done with an AC field of 0.1 Oe in magnitude and 970 Hz in frequency.

mains overdoped at any annealing pressure down to 10^{-5} bar.

It is important to point out that in the case of polycrystalline samples the maximum T_c value of 16.5 K is only reached when annealing at 700°C [31]. In our crystals, a treatment at 700°C and 10^{-3} bar enhances the critical temperature to 15 K (see Fig. 2). However, after this annealing the crystals present no mirror-like surfaces and exhibit broad transitions with widths between 4 and 10 K. Since the Bi2201 phase is at its stability limit at such annealing temperature, these samples are likely to have degraded domains.

Our Bi2201 crystals quantitatively follow the same T_c vs. $P(O_2)$ behavior than polycrystalline samples. This allows us to consider the doping level of our crystals as that obtained by means of thermogravimetric analysis of polycrystalline Bi2201 samples [31] with the same T_c . The evolution of T_c/T_c^{max} with hole-doping is presented in Fig. 3 (b). The data is very well fitted by a parabolic evolution of T_c with p , the number of holes per Cu-O plane, $T_c = T_c^{max}[1 - 82.6(p - p_{OPT})^2]$ [23, 24], yielding $T_c^{max} = 16.5$ K and $p - p_{OPT} = 1.9\delta - 0.23$. Therefore, Bi2201 follows the T_c vs. p relation reported to be obeyed by other single and two-layer cuprates.

Effect of oxygen-doping on the vortex phase diagram of Bi2201

The results presented in this section were obtained in the same sample for two different doping levels within the overdoped regime. The post-annealing treatments

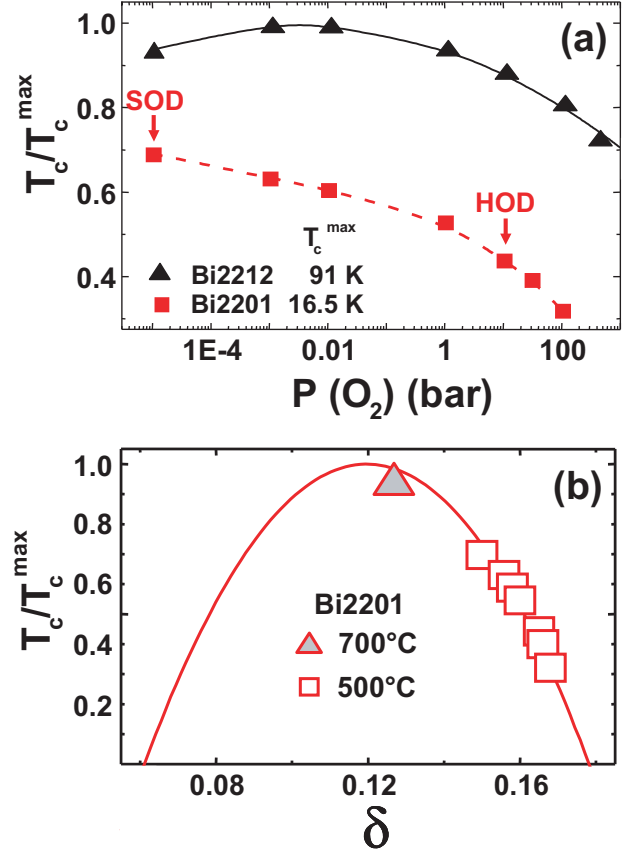


FIG. 3: (a) Normalized critical temperature of our Bi2201 and Bi2212 crystals as a function of the annealing oxygen partial-pressure $P(O_2)$. The annealing treatments were performed at 500°C. In the case of Bi2201 the dotted line is a guide to the eye whereas for Bi2212 the red line is a fit with the relation $T_c = T_c^{max}[1 - 82.6(p - 0.27)^2]$ [23, 24], where $p = 0.011 \ln P(O_2) + 0.3$ [25] is the number of carriers per Cu-O plane. The two doping regimes considered for the study of the doping-evolution of the vortex phase diagram are indicated as slightly(SOD) and highly(HOD)-overdoped. (b) Evolution of T_c/T_c^{max} with oxygen content in our Bi2201 crystals. The doping level was considered as that obtained by means of thermogravimetric analysis of polycrystalline Bi2201 samples [31] having the same T_c as our crystals. The line is a fit to the data with the relation $T_c = T_c^{max}[1 - 82.6(p - p_{OPT})^2]$ yielding $T_c^{max} = 16.5$ K, $p = 1.9\delta$ and $p_{OPT} = 0.23$. A particular annealing treatment performed at 700°C (gray triangle) increased the critical temperature up to 15 K, a value close to the maximum of 16.5 K attributed to optimal doping in Ref. 31.

were performed at 500°C and at pressures of 10^{-5} and 10 bar, resulting in $T_c = (11.4 \pm 0.5)$ and (8.0 ± 0.8) K for the slightly (SOD) and highly-overdoped (HOD) regions, respectively. The doping level corresponds thus to $\delta = 0.15$ for the SOD and 0.165 for the HOD regimes (see Fig. 3 (b)).

The effect of oxygen doping on the vortex phase dia-

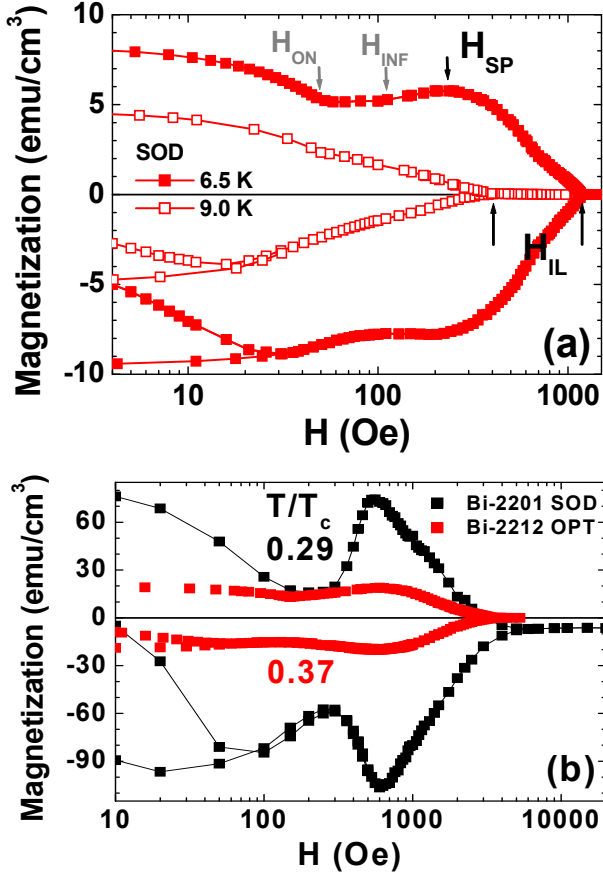


FIG. 4: (a) Magnetization loops of Bi2201 in the slightly-overdoped regime (SOD) [$T_c = (11.4 \pm 0.5)$ K]. The arrows indicate the irreversibility, H_{IL} , and characteristic second-peak fields, H_{SP} (local maximum), H_{ON} (onset), and H_{INF} (inflection or kink point). The measurements were performed at a sweep rate of 10^{-2} Oe/s. (b) Locus of magnetization loops for Bi2201 and Bi2212 (from Ref. 21) at comparable reduced temperatures and doping levels.

gram of Bi2201 was investigated by means of bulk magnetization. The measurements were performed using a MPMS2 SQUID magnetometer, a PPMS measurement system and a vibrating-sample magnetometer (VSM). In the first set of measurements we focus on the doping-evolution of the irreversibility, H_{IL} , and second-peak lines, H_{SP} , H_{ON} and H_{INF} . These lines were obtained from magnetization *vs.* magnetic field measurements, $M(H)$, and from field cooled-zero field cooled (FC-ZFC) temperature-dependent magnetization curves. The magnetic field was applied parallel to the crystal *c*-axis and swept at rates of 10^{-2} Oe/s (SQUID and PPMS magnetometers), 1 and 10 Oe/s (VSM). Figure 4 (a) shows examples of magnetization loops for the SOD regime.

The onset of the irreversible magnetic response was estimated as the field at which the two branches of the magnetization loop merge, as indicated with the arrows in Fig. 4(a). Estimating the irreversibility temperature

from the splitting of the FC-ZFC branches in $M(T)$ curves yielded similar values. Three different effects can be at the origin of an irreversible magnetic response in superconductors: bulk pinning, Bean-Livingston surface barriers [35] and geometrical barriers [36, 37]. The Bean-Livingston surface barrier only produces a significant irreversible behavior in the case of extremely smooth surfaces [38]. In real samples with sharp corners and irregular edges, the effect of this barrier is of lesser importance. In general, macroscopic magnetization measurements are not able to ascertain which of the other two contributions is dominant when measuring an irreversible magnetic response. The effect of geometrical barriers can be revealed by conveniently modifying the sample geometry. In prism-like samples of Bi2212, the geometrical barriers are suppressed and the irreversibility line deviates significantly from the melting line determined by bulk properties [39]. However, for platelet-like Bi2212 samples, independent measurements of the irreversibility and melting lines indicate that both lines incidentally merge [2]. Therefore, in this case, both bulk pinning and geometrical barriers contribute to the irreversible magnetic response at fields lower than H_{IL} . Studying how H_{IL} deviates from the melting line when changing the sample geometry in Bi2201 is far beyond the aim of this work. However, it is reasonable to assume that in our platelet-like samples the effect of bulk pinning may become relevant at fields equal to or slightly lower than $H_{IL}(T)$.

The effect of oxygen-doping on the irreversibility line is shown in the H *vs.* T/T_c phase diagram of Fig. 5. At any temperature, the irreversibility field is enhanced with increasing the oxygen content. A similar evolution of H_{IL} with doping was reported for Bi2212 [21] and Bi2223 [18, 19]. The larger extent of the irreversible vortex solid in the HOD regime indicates that the interlayer coupling is enhanced when δ increases. Therefore, the doping-evolution of H_{IL} suggests a decrease of γ when increasing δ in the overdoped regime.

The second-peak effect is observed in $M(H)$ curves as a peak-valley structure (as also observed in La-doped Bi2201 [40]), see for example the magnetization loops in Fig. 4. The characteristic H_{SP} field associated with the local maximum of the magnetization is clearly evident. However, since in Bi2201 the second-peak feature is broad, the onset and inflection points are poorly resolved. The broad locus of $M(H)$ in Bi2201 is illustrated in Fig. 4(b) by comparing with data obtained in Bi2212 at similar reduced temperatures and doping levels [21]. Our bulk magnetization measurements on Bi2201 detect the second-peak effect within a temperature range $0.18 \leq T/T_c \leq 0.65$. One should notice that the H_{SP} line seems to end below the H_{IL} line. High-resolution local magnetic measurements allowed to study how the H_{SP} line terminates at low fields and high temperatures in the case of YBCO [13]. Our bulk measurements do not enable us to infer anything about the end point of the H_{SP} line.

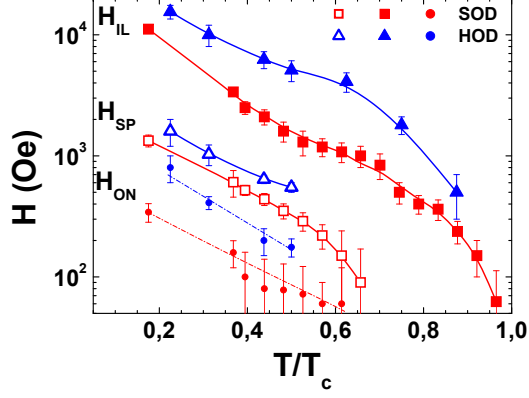


FIG. 5: Vortex phase diagram for the same Bi2201 sample in the slightly (\square SOD) [$T_c = (11.4 \pm 0.5)$ K] and highly-overdoped (\triangle HOD) [$T_c = (8.0 \pm 0.8)$ K] regimes. The irreversibility line, $H_{IL}(T)$ (full symbols, full lines), and the maximum, $H_{SP}(T)$ (open symbols, full lines) and onset lines, $H_{ON}(T)$ (full symbols, dashed lines), of the second-peak effect are shown. The points extracted from magnetization loops correspond to measurements performed at a sweep rate of 10^{-2} Oe/s. The error bars, when not visible, are within the size of the symbols.

As well documented in the literature, the locus of the second-peak effect and eventually its detection might have a dependence on the electric-field level influenced by the magnetic-field sweep-rate. For this reason we have also studied the effect of the sweep rate on the field-location of the characteristic field that we can track with low error, H_{SP} . The magnetization loops shown in Fig. 7 were measured on a slightly-overdoped sample (from the same batch and of the same T_c as the one presented in Fig. 6) at faster sweep rates than that used for the curves presented in Fig. 6 (10^{-2} Oe/s). The right-upper quadrant of the loop is shown for two temperatures, 4.2 and 5 K, and two sweep rates, 10 Oe/s and 1 Oe/s. It is clear from Figs. 6 and 7, that H_{SP} does not depend on the sweep-rate. The differences in the shape of the peak as well as in the apparent H_{IL} of Fig. 7, as compared to Fig. 6, can be due to a lesser doping homogeneity in the larger sample used for the VSM experiment.

The magnetization curves presented in Figs. 6 and 7 indicate an unexpected result for a moderately-doped Bi-based cuprate: unlike the two and three-layer compounds [10, 18, 19], in Bi2201 H_{SP} decreases by one order of magnitude on warming. Both fields H_{ON} and H_{INF} follow a similar trend as shown in the insert of Fig. 6. Because of the still unsolved controversy about which is the true signature of the order-disorder transition [11, 12, 14–17], we will rather discuss the temperature dependence of H_{SP} that we can determine better than H_{ON} and H_{INF} .

The second-peak effect is associated with the vortex-solid order-disorder phase transition at which the elastic energy equals the pinning energy [8, 41]. These two en-

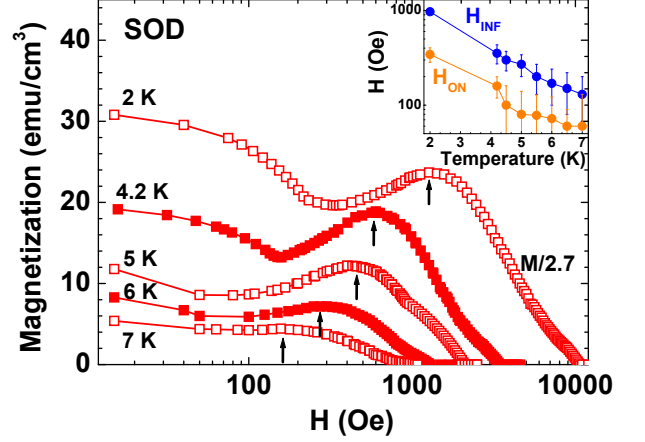


FIG. 6: Upper-right quadrant of the magnetization loops $M(H)$ measured in the SOD regime of Bi2201 [$T_c = (11.4 \pm 0.5)$ K] at different temperatures. The 2 K curve is normalized by a 2.7 factor in order to include all curves in the same scale. A temperature-dependent second-peak effect is detected between 2 and 7 K ($0.18 \leq T/T_c^{max} \leq 0.65$). Arrows indicate the local maxima of the magnetization H_{SP} . Insert: Temperature-evolution of the onset, H_{ON} , and inflection, H_{INF} , characteristic fields of the second-peak feature. Only data up to 7 K are shown since these two fields are not clearly resolved at higher temperatures. The measurements were performed at a sweep rate of 10^{-2} Oe/s.

ergy terms depend on the penetration depth, coherence length and anisotropy of the material, as well as on the temperature-dependent pinning parameter [8]. Considering the two-fluid model [42], $\lambda_{ab}(T)$ and $\xi_{ab}(T)$ vary by only 3% within the temperature range in which the second-peak effect is detected in Bi2201. Such a small variation can not account for the observed temperature-dependent H_{SP} . According to theoretical predictions [8], either a small and/or temperature-dependent anisotropy parameter, or an important temperature-dependent pinning parameter, or both, can produce a non-constant $H_{SP}(T)$.

A temperature-dependent second-peak effect has been reported in several cuprates [12, 14, 43–49]. Roughly, two types of temperature-evolution for H_{SP} are observed. In one class of materials H_{SP} decreases non-monotonically on warming, presenting a valley structure at low temperatures. In this first group, including strongly-doped Bi2212 samples [10, 43, 45–48], the temperature-dependent H_{SP} is associated to enhanced disorder with respect to optimally-doped pure samples. The second class displays a monotonous decrease of the second-peak field on warming, distinctly detected up to temperatures very close to T_c . Notorious examples of cuprates belonging to this group are $\text{YBa}_2\text{Cu}_3\text{O}_{7-\delta}$ [14], $\text{Nd}_{1.85}\text{Ce}_{0.15}\text{CuO}_{4-\delta}$ [44], $\text{HgBa}_2\text{CuO}_{4+\delta}$ [12] and $\text{TlBa}_2\text{CuO}_6$ [49]. In this case the temperature-dependent second-peak effect is associated with the combination of

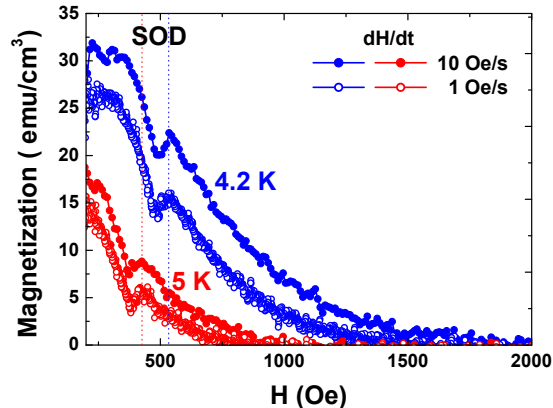


FIG. 7: Upper-right quadrant of the magnetization loops $M(H)$ measured in the SOD regime of Bi2201 [$T_c = (11.4 \pm 0.5) \text{ K}$] at two different sweep rates and temperatures. The field location of the maximum of the second-peak effect is independent of the sweep rate and decreases on warming.

a relatively low anisotropy, a decrease of the pinning energy on warming, and the significant increase of λ and ξ close to T_c .

Since in our pure Bi2201 samples H_{SP} monotonously decreases on warming, the role of disorder is likely to be moderate and this temperature dependence would then be ascribed to a temperature-dependent anisotropy. In order to quantitatively study this issue, the theoretical approach that describes the second-peak effect as the manifestation of an order-disorder phase transition should be considered [8, 41]. However, in our case two reasons hindered us to apply this approach. First, no data on the magnitude of the anisotropy parameter in Bi2201 was previously available in the literature. Second, since it is still controversial which field is the fingerprint of the order-disorder transition [11, 12, 14–17], *local*-magnetization and/or partial magnetization loops data are mandatory. This analysis is beyond the aim of this work. Instead, we directly measured the magnitude of the anisotropy parameter and study its role in the temperature-dependent H_{SP} .

The anisotropy parameter was estimated from directional measurements of the first-penetration field, as previously reported for the Bi2223 compound [19]. Within the London approximation $\gamma = H_{c1}^\perp / H_{c1}^\parallel$ [42], with \perp and \parallel meaning perpendicular and parallel to the ab plane. The sample was aligned in both configurations using a home-made rotation system that reduces the misalignment uncertainty to $\sim 0.5^\circ$. In both configurations the first penetration field H_p was considered as that at which the magnetization shows a detectable relaxation, associated with the entrance of the first vortex. This was done by measuring at every field the relaxation of the magnetic moment during 1 hour. This method reduces the effect of surface and geometrical pinning barriers [50] and is

not affected by the error in identifying H_p from the deviation from linearity in $M(H)$. We assume that in our experiment H_p corresponds to the lower critical field H_{c1} that is borne out by the absence of any asymmetries in the low-temperature hysteresis loops. This confirms that surface pinning effects are negligible. The effect of demagnetizing factors was corrected considering the Meissner slope for both configurations. The large demagnetizing effects strongly reduces the difference between H_p and H_{c1} , thus reducing the uncertainty in measuring the true critical field [51]. In our case, the estimation of the anisotropy parameter from directional measurements of H_{c1} is preferable to that obtained from H_{c2} measurements [50]. The latter are only possible at high fields and/or temperatures, far from the region over which we measured the temperature dependence of H_{SP} .

Figure 8 shows that for SOD Bi2201 γ is strongly temperature-dependent: it increases from roughly 25 to 80 in the temperature-range in which H_{SP} is detected and further increases up to 130 at $T/T_c \sim 0.8$. The data also indicates that Bi2201 presents a moderate-to-high electromagnetic anisotropy in the SOD regime. At low temperatures the anisotropy parameter of SOD Bi2201 is intermediate between that of SOD Bi2223 (~ 20 [19]) and SOD Bi2212 (~ 100 [52]). Local magnetic measurements in moderately-doped Bi2212 revealed that γ increases on warming in the T/T_c range $0.74 - 0.96$ [53].

In the case of Josephson-dominated coupling between the Cu-O planes, $s\gamma < \lambda_{ab}$, the order-disorder transition field is inversely proportional to the anisotropy [54]. Within the temperature range in which H_{SP} is detected in SOD Bi2201, $s\gamma < \lambda_{ab} = (3200 \pm 200) \text{ \AA}$, with $s = 12.3 \text{ \AA}$ [55] the distance between adjacent Cu-O planes. The penetration depth λ_{ab} was obtained by fitting the temperature-dependent H_{c1}^\perp within the London model, considering the two-fluid expression of $\lambda_{ab}(T)$ and $\xi_{ab}(T)$ [56]. Therefore, since in the considered temperature range the Josephson coupling is dominant, the relation $H_{SP} \propto \Phi_0 / (s\gamma)^2$ should be valid. The insert of Fig. 8 shows the excellent agreement between the H_{SP} data and $\propto \Phi_0 / (s\gamma(T))^2$. This finding constitutes a strong evidence that in Bi2201 $H_{SP}(T)$ is governed by the temperature-dependence of the anisotropy and that the pinning parameter is moderate.

This last statement is further supported by critical current data. A less relevant role of disorder implies a reduction on the critical-current density-ratio, J_c/J_0 , with $J_0 = 4c\Phi_0/12\sqrt{3}\pi\lambda_{ab}^2\xi_{ab}$ the depairing-current density. The lower magnitude of J_c in Bi2201, compared to that of Bi2212, is already suggested by the magnetization loops shown in Fig. 4(b). In addition, in Bi2212 a temperature-dependent H_{SP} , attributed to enhanced disorder [45, 48], was only observed for the extremely-overdoped regime in which the critical current is significantly larger than in the optimally-doped regime [52].

The critical current of our Bi2201 crystals is obtained from magnetization loops measured at different temperatures. Considering the Bean model [57], at a

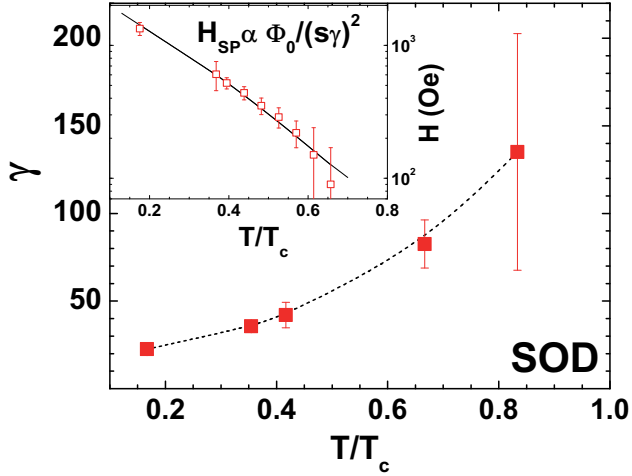


FIG. 8: Temperature-evolution of the anisotropy parameter for slightly-overdoped (SOD) Bi2201 [$T_c = (11.4 \pm 0.5)$ K]. Insert: Fit of the second-peak data with the relation $H_{SP}(T) \propto \Phi_0/(s\gamma(T))^2$ with $\gamma(T)$ estimated from the interpolation of the data in the main panel.

given temperature $J_c(T, H) \sim (3c/2R)\Delta M(T, H)$, where $\Delta M(T, H)$ is the separation between the two branches of the magnetization loop at a field H , c is the speed of light and R is the radius of an equivalent cylindrical sample [57]. Figure 9 shows examples of J_c curves for SOD and HOD Bi2201 at low and high-temperatures. At low temperatures the second-peak effect is clearly observed at intermediate fields and J_c is found to be field-independent at low fields. This suggests that at low temperatures and fields the vortex lines are individually pinned, as also observed in Bi2212 [58] and Bi2223 [19]. At high temperatures the second-peak effect is no longer resolved and the critical current is strongly field-dependent. These findings are observed in both the SOD and HOD regime. Within the temperature-range studied, the critical current density in the HOD is larger than in the SOD regime.

The critical current curves presented in Fig. 9 allow us to estimate that the ratio J_c/J_0 in moderately-overdoped Bi2201 ($J_0(T/T_c = 0.3) \sim 10^3$ A/cm²) is 1-2 orders of magnitude smaller than that of extremely-overdoped Bi2212 [52] at similar reduced-temperatures and fields. Thus the role of disorder in our overdoped Bi2201 samples is much less relevant than in the Bi2212 samples presenting a temperature-dependent H_{SP} [45, 48]. This evidence strengthens our argument that in Bi2201 the observed temperature-dependent second-peak effect is mainly the consequence of an enhancement of anisotropy on warming.

Finally, we would like to discuss another important result evident from the vortex phase diagram presented in Fig. 5: $H_{SP}(T)$ shifts towards higher fields on increasing doping. The same qualitative behavior was reported in Bi2212 [10, 20, 21], Bi2223 [18, 19] and other cuprates [59]. This evolution of $H_{SP}(T)$ is consistent with an en-

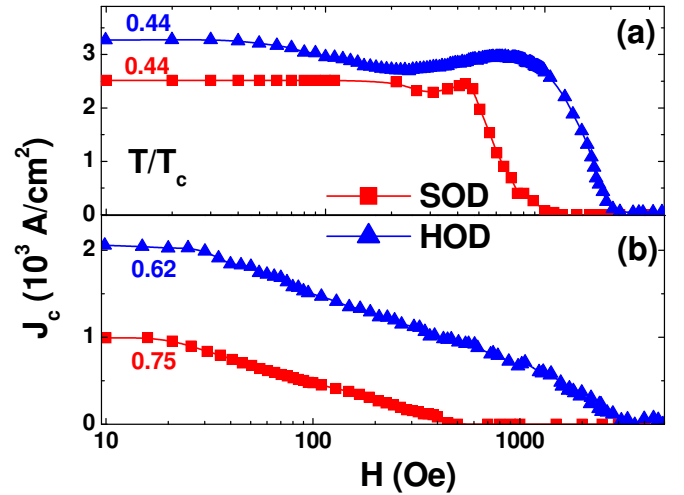


FIG. 9: Critical current density as a function of magnetic field, $J_c(H)$, for slightly (SOD) and highly-overdoped (HOD) Bi2201 obtained from the width of magnetization loops. (a) In the low-temperature data the second-peak is clearly observed whereas (b) in the high-temperature data H_{SP} is no longer resolved.

hancement of coupling between the Cu-O planes with increasing oxygen concentration, as also suggested by the doping dependence of H_{IL} . Since we showed that in Bi2201 H_{SP} is inversely proportional to γ^2 , the doping evolution of $H_{SP}(T)$ allows the estimation of the anisotropy in the HOD regime. Considering the data of Fig. 5 we estimate a 15% decrease of γ for the HOD with respect to the SOD regime.

Conclusions

We have grown pure and large Bi2201 single crystals and tuned the doping level over the whole overdoped regime. The critical temperature of Bi2201 follows a parabolic dependence with the number of holes per Cu-O plane, as found in several single and two-layer cuprates.

The doping-evolution of the vortex phase diagram was studied by means of bulk magnetic measurements. Varying the oxygen concentration affects the vortex phase diagram in a way that is consistent with an enhancement of the coupling between Cu-O layers with increasing δ . This result is in agreement with data reported for the two and three-layer compounds. However, in striking contrast with results found in those compounds, Bi2201 presents a strong temperature-dependent second-peak effect. The electronic anisotropy increases on warming and H_{SP} scales with $1/\gamma^2$, as expected for Josephson-dominated interlayer coupling. Since in addition the relevance of pinning in Bi2201 is smaller than in the other two Bi-based cuprates, we conclude that the temperature-dependent H_{SP} can be mainly ascribed to the temperature evolution of the anisotropy.

This work was supported by the Swiss National Science Foundation, (Project 200020-118029). The authors acknowledge M. Konczykowski for stimulating discussions

and V. Correa for providing us the software version of his published data in Bi2212 [21].

-
- [1] C. Michel, M. Hervieu, M. M. Borel, A. Grandin, F. Deslandes, J. Provost, and B. Raveau, *Z. Phys. B* **68**, 421 (1987).
 - [2] H. Pastoriza, M. F. Goffman, A. Arribère and F. de la Cruz, *Phys. Rev. Lett.* **72**, 2951 (1994).
 - [3] E. Zeldov, D. Majer, M. Konczykowski, V. B. Geshkenbein, V. M. Vinokur, and H. Shtrikman, *Nature* **375**, 373 (1995).
 - [4] P. Kim, Z. Yao, C. A. Bolle, and C. M. Lieber, *Phys. Rev. B* **60**, R12589 (1999).
 - [5] Y. Fasano, M. Menghini, G. Nieva, and F. de la Cruz, *Phys. Rev. B* **62**, 15183 (2000).
 - [6] Y. Fasano, M. De Seta, M. Menghini, H. Pastoriza and F. de la Cruz, *Proceedings of the National Academy of Sciences (PNAS)* **102**, 3898 (2005).
 - [7] T. Nattermann, *Phys. Rev. Lett.* **64**, 2454 (1990).
 - [8] T. Giamarchi and P. LeDoussal, *Phys. Rev. Lett.* **72**, 1530 (1994).
 - [9] D. S. Fisher, M. P. A. Fisher and D. A. Huse, *Phys. Rev. B* **43**, 130 (1991).
 - [10] B. Khaykovich, E. Zeldov, D. Majer, T. W. Li, P. H. Kes and M. Konczykowski, *Phys. Rev. Lett.* **76**, 2555 (1996).
 - [11] G. Ravikumar, H. Küpfer, A. Will, R. Meier-Hirmer, and Th. Wolf, *Phys. Rev. B* **65**, 094507 (2002).
 - [12] D. Stamopoulos and M. Pissas, *Phys. Rev. B* **65**, 134524 (2002).
 - [13] D. Stamopoulos, M. Pissas and A. Bondarenko, *Phys. Rev. B* **66**, 214521 (2002).
 - [14] D. Giller, A. Shaulov, Y. Yeshurun and J. Giapintzakis, *Phys. Rev. B* **60**, 106 (1999).
 - [15] T. Nishizaki, T. Naito, S. Okayasu, A. Iwase and N. Kobayashi, *Phys. Rev. B* **61**, 3649 (2000).
 - [16] Y. Radzyner, S. B. Roy, D. Giller, Y. Wolfus, A. Shaulov, P. Chaddah, and Y. Yeshurun, *Phys. Rev. B* **61**, 14362 (2000).
 - [17] M. Pissas, E. Moraitakis, G. Kallias, and A. Bondarenko, *Phys. Rev. B* **62**, 1446 (2000).
 - [18] A. Piriou, Y. Fasano, E. Giannini and Ø. Fischer, *Physica C* **460-462**, 408 (2007).
 - [19] A. Piriou, Y. Fasano, E. Giannini and Ø. Fischer, *Phys. Rev. B* **77**, 184508 (2008).
 - [20] K. Kishio *et al.*, in *Proceedings of the 7th International Workshop on Critical Currents in Superconductors*, edited by H. W. Weber (World Scientific, Singapore, 1994), p.339; C. Bernhard, C. Wenger, Ch. Niedermayer, D. M. Pooke, J. L. Tallon, Y. Kotaka, J. Shimoyama, K. Kishio, D. R. Noakes, C. E. Stronach, T. Sembiring and E. J. Ansaldo, *Phys. Rev. B* **52**, R7050 (1995); C. M. Aegerter, S. L. Lee, H. Keller, E. M. Forgan, S. H. Lloyd, *Phys. Rev. B* **54**, R15661 (1996); T. Tamegai *et al.*, in *Proceedings of the 9th International Symposium on Superconductivity*, edited by S. Nakajima and M. Murakami (Springer-Verlag, Tokyo, 1997), p.621.
 - [21] V. F. Correa, E. E. Kaul, G. Nieva, *Phys. Rev. B* **63**, 172505 (2001).
 - [22] K. Kishio, in *Coherence in High Temperature Superconductors*, edited by G. Deutscher and A. Revcolevschi (World Scientific, Singapore, 1996), p. 212, and references therein.
 - [23] C. Allgeier and J. S. Schilling, *Physica C* **168**, 499 (1990).
 - [24] M. R. Presland, J. L. Tallon, R. G. Buckley, R. S. Liu, and N. E. Flower, *Phys. C* **176**, 95 (1991).
 - [25] X. Zhao, X. Sun, X. Fan, W. Wu, X.-G. Li, S. Guo and Z. Zhao, *Physica C* **307**, 265 (1998).
 - [26] J. M. Tarascon, W. R. McKinnon, Y. LePage, K. Remschnig, R. Ramesh, R. Jones, G. Pleizier, and G. W. Hull, *Phys. C* **172**, 13 (1990).
 - [27] A. E. Schloegl, J. J. Neumeier, J. Diederichs, C. Allgeier, J. S. Schilling, and W. Yelon, *Phys. C* **216**, 417 (1993).
 - [28] N. R. Khasanova, E. V. Antipov, *Physica C* **246**, 241 (1995).
 - [29] J. Zhang, C. Zhang, H. Xie, and Y. Zhang, *J. Cryst. Growth* **222**, 518 (2001).
 - [30] H. Eisaki, N. Kaneko, D. L. Feng, A. Damascelli, P. K. Mang, K. M. Shen, Z. -X. Shen, and M. Greven, *Phys. Rev. B* **69**, 064512 (2004).
 - [31] F. Jean, D. Colson, G. Collin, N. Blanchard, Z. Konstantinovic, G. Le Bras, A. Forget, and M. Andrieux, *Phys. Rev. B* **68**, 174511 (2003).
 - [32] B. Liang, A. Maljuk, and C. T. Lin, *Phys. C* **361**, 156 (2001).
 - [33] H. Luo, L. Fang, G. Mu, and H.-H. Wen, *J. Cryst. Growth* **305**, 222-227 (2007).
 - [34] E. Giannini, V. Garnier, R. Gladyshevskii and R. Flukiger, *Supercond. Sci. Technol.* **17**, 220 (2004).
 - [35] C. P. Bean and J. D. Livingston, *Phys. Rev. Lett.* **12**, 14 (1964).
 - [36] E. Zeldov *et al.*, *Phys. Rev. Lett.* **73**, 1428 (1994).
 - [37] M. V. Indenbom, and E. H. Brandt, *Phys. Rev. Lett.* **73**, 1731 (1994).
 - [38] P. G. de Gennes, *Superconductivity of Metals and Alloys* (Benjamin, New York, 1966).
 - [39] D. Majer, E. Zeldov and M. Konczykowski, *Phys. Rev. Lett.* **75**, 1166 (1995).
 - [40] T. Amano *et al.*, *Phys. C* **408** (2004).
 - [41] D. Ertas and D. R. Nelson, *Physica C* **272**, 79 (1996); T. Giamarchi and P. LeDoussal, *Phys. Rev. B* **55**, 6577 (1997); V. Vinokur, B. Khaykovich, E. Zeldov, M. Konczykowski, R. A. Doyle and P. Kes, *Physica C* **295**, 209 (1998); J. Kierfeld, *Physica C* **300**, 171 (1998).
 - [42] G. Blatter, M. V. Feigelman, V. B. Geshkenbein, A. I. Larkin and V. M. Vinokur, *Rev. Mod. Phys.* **66**, 1125 (1994).
 - [43] S. Ooi, T. Tamegai, and T. Shibauchi, *Physica C* **259**, 280 (1996).
 - [44] D. Giller, A. Shaulov, R. Prozorov, Y. Abulafia, Y. Wolfus, L. Burlachkov, Y. Yeshurun, E. Zeldov, V. M. Vinokur, J. L. Peng, and R. L. Greene, *Phys. Rev. Lett.* **79**, 2542 (1997).
 - [45] S. Ooi, T. Shibauchi and T. Tamegai, *Physica C* **302**, 339 (1998).

- [46] A. Mumtaz, Y. Yamaguchi, K. Oka and G. Rajaram, *Physica C*, **302**, 331-338 (1998).
- [47] M. Baziljevich, D. Giller, M. McElfresh, Y. Abulafia, Y. Radzyner, J. Schneck, T. H. Johansen, and Y. Yeshurun, *Phys. Rev. B* **62**, 4058 (2000)
- [48] D. Darminto, M. Diantoro, I. M. Sutjahja, A. A. Nugroho, W. Loeksmanto, and M. O. Tjia, *Physica C* **378-381**, 479 (2002).
- [49] P. Chowdhury, Heon-Jung Kim, S. K. Gupta and Sung-Ik Lee, *J. Phys.: Condens. Matter* **16**, 6727 (2004).
- [50] M. Nideröst, R. Frassanito, M. Saalfrank, A. C. Mota, G. Blatter, V. N. Zavaritsky, T. W. Li, and P. H. Kes, *Phys. Rev. Lett.* **81**, 3231 (1998).
- [51] L. Burlachkov, *Phys. Rev. B* **47**, 8056 (1993).
- [52] V. F. Correa, J. A. Herbsommer, E. E. Kaul, F. de la Cruz and G. Nieva, *Phys. Rev. B* **63**, 092502 (2001).
- [53] M. Konczykowski, C. J. van der Beek, A.E. Koshelev, V. Mosser, M. Dodgson and P. H. Kes, *Phys. Rev. Lett.* **97**, 237005 (2006).
- [54] A. E. Koshelev, V.M. Vinokur, *Phys. Rev. B* **57**, 8026 (1998).
- [55] S.I. Vedeneev, A.G.M. Jansen, E. Haanappel, P. Wyder, *Phys. Rev. B*, **60**, 12467 (1999).
- [56] In order to calculate $\xi_{ab}(T)$ we have taken $\xi_{ab}(0) = 40 \text{ \AA}$ according to Ref. 55.
- [57] C. P. Bean, *Rev. Mod. Phys.* **36**, 31 (1964).
- [58] V.F. Correa, G. Nieva, F. de la Cruz, *Phys. Rev. Lett.* **87**, 057003 (2001).
- [59] V. Hardy, A. Wahl, A. Ruyter, A. Maignan, C. Martin, L. Coudrier, J. Provost, Ch. Simon, *Physica C* **232**, 347 (1994); K. Shibata, T. Nishizaki, T. Sasaki and N. Kobayashi, *Phys. Rev. B* **66**, 214518 (2002); T. Masui, Y. Takano, K. Yoshida, K. Kajita and S. Tajima, *Physica C* **412-414** 515 (2004).